光学学报

低远场发散角976 nm基横模脊形半导体激光器

王振诺[1,2]，仲莉[1,2*]，张德帅[1,2**]，刘素平[1]，潘智鹏[1,2]，常津源[1,2]，何天将[1,2]，马骁宇[1,2]

[1]中国科学院半导体研究所光电子器件国家工程研究中心，北京 100083；

[2]中国科学院大学材料科学与光电技术学院，北京 100049

摘要 采用非对称大光腔外延结构设计制备出976 nm InGaAs/GaAsP应变补偿量子阱脊形半导体激光器，通过对外延结构的设计优化，以实现器件低远场发散角、低功耗的基横模稳定输出。所制备基横模脊形半导体激光器的脊宽为5 μm、腔长为1500 μm，在25 ℃测试温度下，可获得422 mW最大连续输出功率，峰值波长为973.3 nm，光谱线宽(FWHM)为1.4 nm。当注入电流为500 mA时，垂直和水平远场发散角(FWHM)分别为24.15°和3.90°。在15～35 ℃测试温度范围内对脊形半导体激光器的水平远场发散角进行测试分析，发现随着测试温度的升高，器件远场分布变化较小，水平远场发散角基本维持在3.9°左右。

关键词 激光器；976 nm半导体激光器；基横模脊形波导；低远场发散角；非对称大光腔结构

中图分类号 TN248.4 **文献标志码** A **DOI：** 10.3788/AOS231905

1 引 言

976 nm半导体激光器作为固体激光器、光纤激光器及光纤放大器的主要泵浦光源，在工业加工、医疗、通信等领域得到了广泛应用[1-5]。作为掺铒光纤放大器的重要泵浦光源，976 nm基横模半导体激光器可以实现与光纤的高效率耦合，提升光纤放大器输出性能，有效降低光纤放大器使用成本，这对于拓展掺铒光纤放大器在光纤通信等领域的应用起到了重要作用[6-7]。近些年，随着半导体激光器制备工艺的提升，976 nm波段基横模半导体激光器在低电流注入水平下的输出功率已达百毫瓦量级。陈烨[8]制备出脊宽为3.5 μm、腔长为800 μm的980 nm基横模脊形半导体激光器。该器件采用大光腔结构，通过优化波导层厚度至0.85 μm，以获得低远场发散角，同时对限制层材料组分和厚度进行优化设计以降低载流子泄漏、电流扩展和串联电阻等因素对器件转换效率及阈值电流密度的影响。在室温条件下，该激光器可获得超过140 mW输出光功率；在100 mA工作电流下，该激光器的垂直远场发散角为28°，水平远场发散角为6.9°。Liu等[9]制备出脊宽为4 μm、腔长为900 μm的980 nm基横模脊形半导体激光器。该器件采用波导层总厚度为0.8 μm的大光腔结构，相较于常见波导层总厚度为0.1～0.2 μm的外延结构，大光腔结构有效降低出光腔面的光功率密度，有利于提高器件可靠性且保持较小的远场发散角度；在23 ℃、620 mA连续注入条件下，可以获得500 mW输出光功率，垂直远场发散角(FWHM)为30°。刘军等[10]以脊宽为3 μm、腔长为3000 μm的980 nm基横模脊形半导体激光器获得600 mW的单模输出，该器件同样采用大光腔结构，将波导层总厚度增加至0.5 μm，较大程度上增加了输出光束的近场光斑尺寸，进而实现低远场发散角，垂直和水平方向的远场发散角分别为40°和8°，这就满足了半导体激光器所泵浦掺铒光纤放大器在光纤通信领域中的大多数应用需求[11]。受到器件本身结构限制，脊形半导体激光器仍具有较大的远场发散角，这就限制了器件与光纤之间的耦合效率。因此，进一步降低976 nm基横模半导体激光器的远场发散角，对提升掺铒光纤放大器产品性能具有重要的现实意义[12]。目前，为降低器件远场发散角度，提高转换效率等输出性能，宽条形半导体激光器领域已开始使用非对称大光腔外延结构，该结构中波导层总厚度已提升至2 μm[13-14]。

本文通过对外延结构进行优化设计，制备出一种低远场发散角、低功耗的976 nm基横模脊形半导体激光器，并对器件的输出功率、激射光谱、远场发散角等性能参数进行测试分析，探讨了不同测试温度对器件输出性能的影响。

2 器件设计优化

为实现脊形半导体激光器低功耗、低远场发散角的输出特性，通常对器件外延结构进行优化。为获得

收稿日期：2023-12-11；**修回日期**：2024-01-22；**录用日期**：2024-02-02；**网络首发日期**：2024-02-20

通信作者：*zhongli@semi.ac.cn；**zhangdeshuai@semi.ac.cn

较高的转换效率，976 nm半导体激光器一般采用InGaAs材料作为压应变量子阱层，根据所需激射波长对量子阱材料中In组分含量和量子阱厚度进行优化设计。为进一步提高器件性能，本文在InGaAs量子阱两侧加入GaAsP材料作为势垒层。GaAsP作为宽禁带宽度材料，可与InGaAs量子阱产生较大的带阶，有利于限制量子阱中载流子向波导层泄漏，进而提高器件转换效率。同时，GaAsP可作为张应变势垒层对InGaAs压应变量子阱进行应变补偿，可有效降低外延生长量子阱过程中由应变导致的缺陷，提高半导体激光器的可靠性[15]。器件整体外延结构采用非对称大光腔结构，通过增加波导层厚度来实现大光腔设计，以延展器件近场光斑尺寸，降低远场发散角度，并且较大的波导层厚度将有助于增加器件出光面积，增大腔面光学灾变性损伤阈值[13]；同时，对P侧和N侧波导层厚度进行优化设计，通过减小P侧波导层厚度，实现光场向N侧偏移，以减小P侧掺杂区产生的光吸收损耗，降低P侧波导层电阻和电流损耗的影响，提高器件转换效率[14,16]。在外延结构中，还需要对各层结构的掺杂浓度进行优化。为降低器件的腔内损耗，波导层通常采用未掺杂材料，但这也将增大器件的串联电阻，影响输出性能。为此，对限制层掺杂浓度进行优化，以降低器件的串联电阻，减小腔内损耗，实现脊形半导体激光器的高效率输出[17]。经过理论计算和实验探索，本实验采用表1所示的外延结构参数。图1所示为所用外延结构沿外延方向的折射率分布和光场分布。

表1　脊形半导体激光器外延结构参数

Table 1　Epitaxial structure parameters of ridge diode laser

Layer order	Layer	Material	Thickness /μm	Doped concentration /cm^{-3}
9	Ohmic contact	GaAs	0.2	C: 1×10^{20}
8	Upper confinement	Al$_{0.4}$GaAs	0.7	C: 1×10^{18}
7	Upper waveguide	Al$_{0.15}$GaAs	0.7	Undoped
6	Upper transition	Al$_{0.1}$GaAs	0.04	Undoped
5	Active region	InGaAs/GaAsP	—	Undoped
4	Lower transition	Al$_{0.1}$GaAs	0.04	Undoped
3	Lower waveguide	Al$_{0.15}$GaAs	1.6	Undoped
2	Lower confinement	Al$_{0.4}$GaAs	0.8	Si: 5×10^{17}
1	Buffer layer	GaAs	0.5	Si: 1×10^{18}
0	Substrate	GaAs	—	—

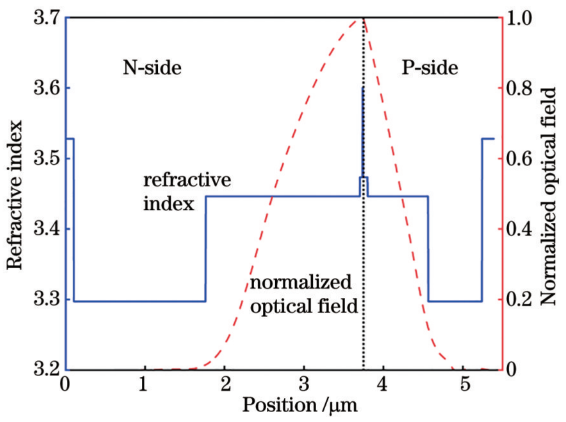

图1　半导体激光器外延结构折射率和归一化光场分布

Fig. 1　Refractive index and normalized optical field distribution of diode laser epitaxial structure

为实现脊形半导体激光器基横模稳定输出，通常利用基横模截止条件获得脊形波导结构宽度和深度的最优关系[18-19]，表达式为

$$w^2=\frac{\lambda^2}{4\left(n_{\mathrm{eff2}}^2-n_{\mathrm{eff1}}^2\right)},\tag{1}$$

式中：w为脊形波导宽度；λ为激射波长；n_{eff2}为脊形台面的有效折射率；n_{eff1}为脊形两侧刻蚀区域的有效折射率。由式(1)可知：当脊形台面宽度增大时，脊形台面及两侧区域的有效折射率差减小，意味着脊形两侧区域刻蚀深度减小，将导致脊形波导对光场的限制能力减弱，载流子扩散效应增强，致使器件转换效率下降；当脊形台面宽度减小时，脊形两侧区域的刻蚀深度增加，侧向限制作用增强，而脊形宽度过小则容易导致高阶模式激射，且会限制出光面积，易于造成腔面光学灾变性损伤[17]。因此，本文选择的脊形波导宽度为5 μm，相应的脊形两侧区域的深度为0.85 μm，其光场分布如图2所示。

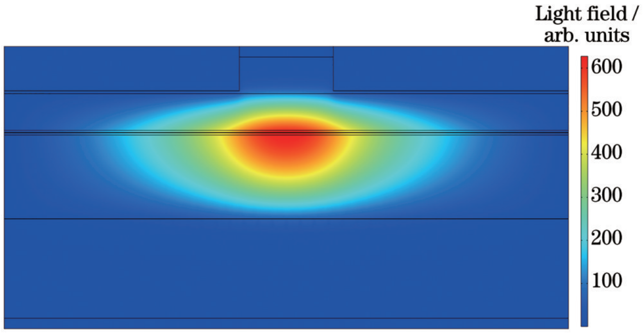

图2　脊形波导光场分布

Fig. 2　Light field distribution of ridge waveguide

3 实验制备及结果讨论

采用金属有机物化学气相沉积设备在N型GaAs衬底上进行外延结构生长，外延结构参数如表1所示。首先，采用光刻、刻蚀等工艺在外延片表面制备出脊宽为5 μm、脊深为0.85 μm的脊形波导结构；其次，利用等离子体增强化学气相沉积设备在外延片表面沉积SiO_2材料作为电绝缘层，并在脊形波导上刻蚀出电极注入窗口，利用磁控溅射设备溅射Ti/Pt/Au金属电极；然后，经减薄抛光后在N面真空蒸镀Au/Ge/Ni型金属电极，经过解理制备出腔长为1500 μm的脊形半导体激光器，并通过镀膜工艺在器件前腔面镀增透膜，反射率为4%，在后腔面镀高反膜，反射率为97%；最后，经过烧焊、引线压焊等工艺将激光器芯片焊接到AlN陶瓷热沉上。

3.1 电光特性

在激光器芯片制备封装之后，将测试温度控制在25 ℃，对器件输出性能进行测试分析。图3为脊形半导体激光器的功率-电流-电压（*P*-*I*-*V*）特性曲线。从测试数据可以得到，脊形半导体激光器的阈值电流约为51.2 mA。当注入电流高于阈值电流时，半导体激光器内产生的增益可以弥补激光器腔体产生的各项损耗，半导体激光器内部光子实现净放大，使得半导体激光器处于受激发射状态，从而产生激光辐射。当注入电流达到550 mA时，半导体激光器获得的最大连续输出功率为422 mW，且没有出现明显的热饱和现象；当注入电流超过550 mA时，功率曲线扭曲，出现kink现象。这是因为在高注入电流条件下，受到半导体激光器自热效应的影响，器件内部出现明显的热透镜效应，产生高阶横模，从而影响输出功率。在注入电流低于550 mA时重复测试，半导体激光器仍能实现较为稳定的基横模输出，在注入电流为500 mA时，可以获得53.6%的最大电光转换效率，实现了较高效率的注入电能向输出光能的转换。

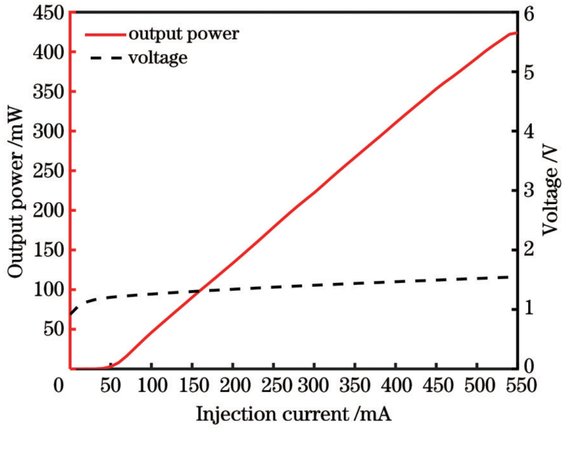

图3 脊形半导体激光器的*P*-*I*-*V*特性曲线

Fig. 3 *P*-*I*-*V* characteristic curves of ridge diode laser

图4所示为脊形半导体激光器的激射光谱。在测试温度为25 ℃的条件下，当输出功率为422 W时，半导体激光器的峰值波长为973.3 nm，相应的光谱线宽（FWHM）为1.4 nm。较窄的光谱线宽可以更好地对应光纤放大器中离子的吸收峰，为光纤放大器提供更好的泵浦性能。

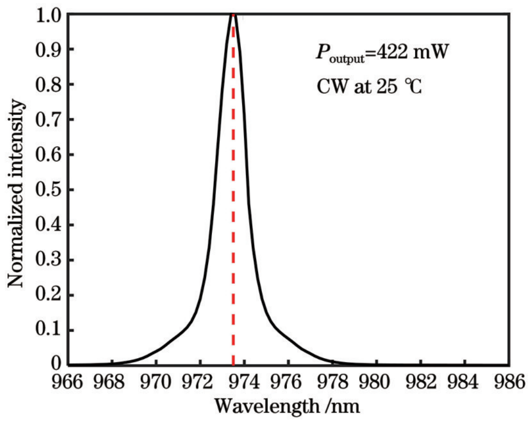

图4 最大输出功率下脊形半导体激光器的激射光谱

Fig. 4 Emission spectrum of ridge diode laser at maximum output power

图5所示为25 ℃测试温度条件下，注入电流为500 mA、输出功率为377 mW时，垂直于PN结方向和平行于PN结方向的远场分布。当连续输出功率为377 mW时，垂直远场发散角（FWHM）为24.15°，水平远场发散角（FWHM）为3.90°。器件在垂直方向采用较厚的波导层结构，扩展了外延结构中的光场分布，从而减小垂直远场发散角[20]。从图5可以明显看出，在500 mA连续工作电流下，水平远场分布图呈现良好的高斯线型，表明所制备的脊形半导体激光器具有良好的基横模特性，有利于提高半导体激光器和光纤之间的耦合效率。

图6所示为25 ℃测试温度条件下，注入电流分别为300、400、500 mA时的水平远场强度分布。由图6可知：在300、400、500 mA 3种注入电流下，水平远场

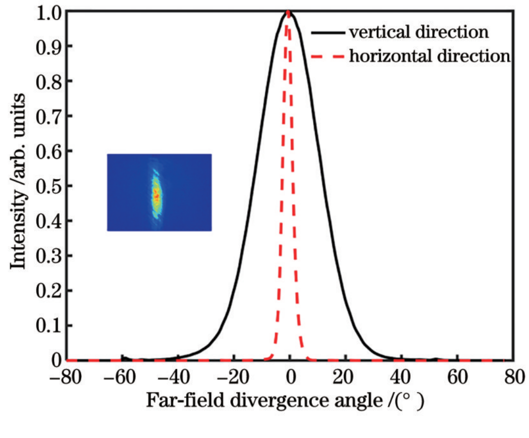

图5 脊形半导体激光器远场强度分布

Fig. 5 Far-field intensity distribution of ridge diode laser

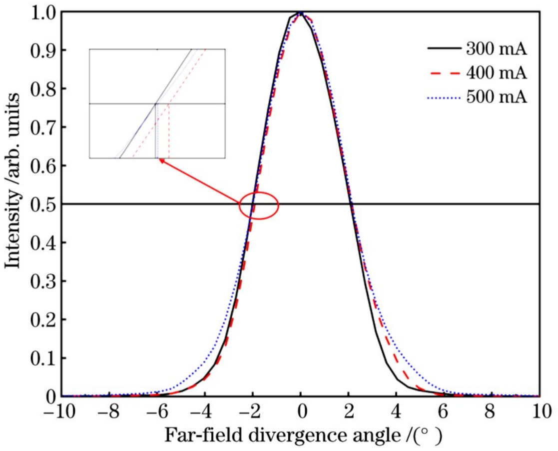

图 6　不同注入电流下脊形半导体激光器的水平远场强度分布

Fig. 6　Horizontal far-field intensity distribution of ridge diode laser under different injection currents

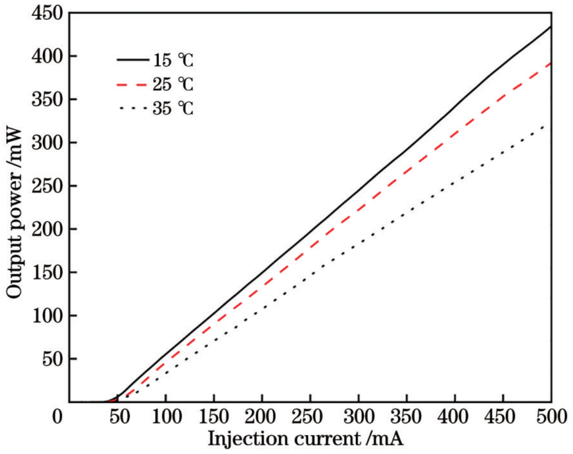

图 7　不同工作温度下脊形半导体激光器的 P-I 特性

Fig. 7　P-I characteristics of ridge diode laser at different operating temperatures

发散角（FWHM）分别为3.75°、3.80°和3.90°；随着注入电流不断增加，水平远场发散角呈现增大的趋势。这是因为在增大注入电流的过程中，半导体激光器输出功率增大，器件内部自热效应也增强，从而导致热透镜效应加剧，远场发散角逐渐增大。由于器件主要在低电流注入水平下工作，自热效应的影响相对较小，因此该器件水平远场发散角在不同注入电流下的变化较小，可以维持在低于4°水平。

3.2　温度特性

通常情况下，随着工作温度的不断增加，半导体激光器的输出性能会逐渐衰退。一般使用特征温度对半导体激光器的温度稳定性进行判定，其可通过不同工作温度下的阈值电流求得，其相关公式[21]为

$$I_{\mathrm{th}}(T_2)=I_{\mathrm{th}}(T_1)\cdot\exp\left[\left(T_2-T_1\right)/T_0\right],\qquad(2)$$

式中：$I_{\mathrm{th}}(T_1)$和$I_{\mathrm{th}}(T_2)$分别为T_1和T_2工作温度下的阈值电流；T_0为特征温度。从式（2）可以看出，特征温度越高，不同工作温度下阈值电流的变化量越小，半导体激光器的温度稳定性就越好。因此，本文对半导体激光器在不同工作温度下的输出性能进行测试分析。

图7所示为15、25、35 ℃ 3种工作温度下脊形半导体激光器的功率-电流（P-I）特性曲线。当工作电流为500 mA时，15、25、35 ℃ 3种工作温度下器件的连续输出功率分别为434、377、302 mW，相应的阈值电流分别为48.7、51.2、54.6 mA，随着工作温度升高，器件阈值电流逐渐增大。这是因为半导体激光器工作温度升高，有源区域内载流子泄漏增多，从而减小了有源区内注入电流产生的载流子密度，降低了发光效率，进而使得器件阈值电流增加、输出功率降低。随后，利用式（2）对半导体激光器的特征温度进行计算，得到特征温度T_0约为194 K。相对较大的特征温度很好地说明了所制备的脊形半导体激光器具有良好的温度稳定性。这是因为在InGaAs量子阱两侧增加高禁带宽度的GaAsP材料作为势垒层，两种材料之间具有较大的带阶，可以更好地抑制量子阱中载流子泄漏，提高注入电流利用率，提升发光效率。

图8所示为连续注入电流为500 mA条件下，15、25、35 ℃ 3种工作温度对应的器件水平远场强度分布。从图8可以看到：当工作温度分别为15、25、35 ℃时，水平远场发散角（FWHM）分别为3.45°、3.90°和3.90°；随着工作温度逐渐升高，水平远场发散角不断增大。这是因为在实际工作过程中，半导体激光器受到自热效应的影响，内部温度分布不均匀，产生热透镜效应，各层外延材料的折射率发生变化，并在器件内部形成折射率导引，从而造成光场分布变化。此外，工作温度的上升加剧了半导体激光器内部的热透镜效应，使得远场发散角逐渐增大，但器件在相对较高的工作温度下仍能保持较小的水平远场发散角，这将有利于提高其在光泵浦应用中的耦合效率。

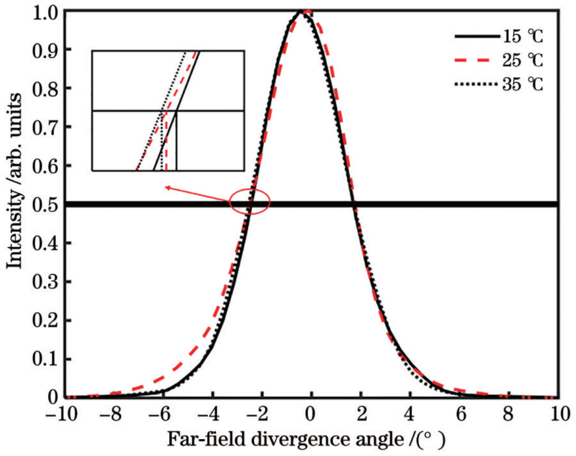

图 8　不同工作温度下脊形半导体激光器的水平远场强度分布

Fig. 8　Horizontal far-field intensity distribution of ridge diode laser at different temperatures

4 结论

为提高脊形半导体激光器的输出性能，从外延结构入手，采用非对称大光腔外延结构，并在InGaAs压应变量子阱两侧引入高禁带GaAsP材料作为张应变势垒，制备出脊宽为5 μm、腔长为1500 μm的976 nm应变补偿低远场、低功耗基横模脊形半导体激光器。在25 ℃测试温度下，当阈值电流为51.2 mA、注入电流为550 mA时，最大连续输出功率（422 mW）的峰值波长为973.3 nm，光谱线宽（FWHM）为1.4 nm。当注入电流为500 mA时，垂直和水平远场发散角（FWHM）分别为24.15°和3.90°。对不同测试温度下半导体激光器的远场分布进行测试分析，发现随着测试温度升高，器件远场分布变化较小，可以保持较小的远场发散角度。

参考文献

[1] Gordeev N Y, Maximov M V, Zhukov A E. Transverse mode tailoring in diode lasers based on coupled large optical cavities[J]. Laser Physics, 2017, 27(8): 086201.

[2] Gordeev N Y, Payusov A S, Shernyakov Y M, et al. Transverse mode competition in narrow-ridge diode lasers[J]. Laser Physics, 2019, 29(2): 025003.

[3] Karow M M, Frevert C, Platz R, et al. Efficient 600-W-laser bars for long-pulse pump applications at 940 and 975 nm[J]. IEEE Photonics Technology Letters, 2017, 29(19): 1683-1686.

[4] 陈芬, 崔碧峰, 冯靖宇, 等. 大功率半导体激光器光束质量的研究与进展[J]. 激光与光电子学进展, 2023, 60(21): 2100002.
Chen F, Cui B F, Feng J Y, et al. Research and progress of high-power semiconductor lasers with high beam quality[J]. Laser & Optoelectronics Progress, 2023, 60(21): 2100002.

[5] 黄宁博, 吴远大. 高线性波分复用模拟光链路的设计及实现[J]. 激光与光电子学进展, 2023, 60(5): 0506005.
Huang N B, Wu Y D. Design and implementation of high-linearity wavelength division multiplexing analog optical link[J]. Laser & Optoelectronics Progress, 2023, 60(5): 0506005.

[6] Harding C M, Chen Y C, Dalby R J. Low-divergence single-mode ridge waveguide diode lasers[J]. IEEE Photonics Technology Letters, 1991, 3(3): 199-201.

[7] Hempel M, Tomm J W, Elsaesser T, et al. Analysis of 980 nm emitting single-spatial mode diode lasers at high power levels by complementary imaging techniques[J]. Proceedings of SPIE, 2015, 9348: 93480N.

[8] 陈烨. 高功率980 nm单模脊形量子阱半导体激光器的研究[D]. 长春: 长春理工大学, 2009: 20-28.
Chen Y. A examination on high power 980 nm single-mode ridge quantum well semiconductor lasers[D]. Changchun: Changchun University of Science and Technology, 2009: 20-28.

[9] Liu B, Liu Y Y. High power 980 nm ridge waveguide semiconductor laser diode[J]. Laser & Optoelectronics Progress, 2015, 52(9): 091404.

[10] 刘军, 李伯中, 陈芳, 等. 400 mW 980 nm泵浦激光器设计[J]. 光通信研究, 2023(2): 63-68.
Liu J, Li B Z, Chen F, et al. The 980 nm pump laser with output power of 400 mW[J]. Study on Optical Communications, 2023(2): 63-68.

[11] Yang G, Wong V, Rossin V, et al. Grating stabilized high power 980 nm pump modules[C]//2007 Conference on Optical Fiber Communication and the National Fiber Optic Engineers Conference, March 25–29, 2007, Anaheim, CA, USA. New York: IEEE Press, 2007.

[12] Sabourdy D, Desfarges-Berthelemot A, Kermene V, et al. 975-nm single-mode laser source: external coherent combining of two pigtailed laser diodes[J]. IEEE Journal of Selected Topics in Quantum Electronics, 2004, 10(5): 1033-1038.

[13] Crump P, Erbert G, Wenzel H, et al. Efficient high-power laser diodes[J]. IEEE Journal of Selected Topics in Quantum Electronics, 2013, 19(4): 1501211.

[14] Kaul T, Erbert G, Maassdorf A, et al. Extreme triple asymmetric (ETAS) epitaxial designs for increased efficiency at high powers in 9xx-nm diode lasers[J]. Proceedings of SPIE, 2018, 10514: 105140A.

[15] 袁庆贺, 井红旗, 仲莉, 等. 高功率高可靠性9XX nm激光二极管[J]. 中国激光, 2020, 47(4): 0401006.
Yuan Q H, Jing H Q, Zhong L, et al. High-power and high-reliability 9XX-nm laser diode[J]. Chinese Journal of Lasers, 2020, 47(4): 0401006.

[16] 周坤, 何林安, 李弋, 等. 高功率793 nm半导体激光器[J]. 红外与毫米波学报, 2022, 41(4): 685-689.
Zhou K, He L A, Li Y, et al. High power 793 nm diode lasers[J]. Journal of Infrared and Millimeter Waves, 2022, 41(4): 685-689.

[17] 付鹏, 张艳春, 赵涛, 等. 高效率高功率976 nm半导体激光芯片设计与制备[J/OL]. 中国激光: 1-13[2024-01-18]. http://kns.cnki.net/kcms/detail/31.1339.tn.20231114.1001.002.html.
Fu P, Zhang Y C, Zhao T, et al. Design and fabrication of high-efficiency and high-power 976 nm semiconductor laser chips [J/OL]. Chinese Journal of Lasers: 1-13[2024-01-18]. http://kns.cnki.net/kcms/detail/31.1339.tn.20231114.1001.002.html.

[18] 常津源, 熊聪, 祁琼, 等. 1550 nm高功率基横模半导体激光器及温度特性[J]. 光学学报, 2023, 43(7): 0714003.
Chang J Y, Xiong C, Qi Q, et al. 1550 nm high-power fundamental transverse mode semiconductor laser and its temperature characteristics[J]. Acta Optica Sinica, 2023, 43(7): 0714003.

[19] 张娜玲, 井红旗, 袁庆贺, 等. 高功率1060 nm锥形激光器[J]. 光学学报, 2022, 42(5): 0514002.
Zhang N L, Jing H Q, Yuan Q H, et al. High power 1060 nm tapered laser[J]. Acta Optica Sinica, 2022, 42(5): 0514002.

[20] Crump P, Pietrzak A, Bugge F, et al. 975 nm high power diode lasers with high efficiency and narrow vertical far field enabled by low index quantum barriers[J]. Applied Physics Letters, 2010, 96(13): 131110.

[21] Akahane K, Yamamoto N, Kawanishi T. High characteristic temperature of highly stacked quantum-dot laser for 1.55-μm band[J]. IEEE Photonics Technology Letters, 2010, 22(2): 103-105.

976 nm Fundamental Transverse Mode Ridge Diode Laser with Narrow Far-Field Divergence Angle

Wang Zhennuo[1,2], Zhong Li[1,2*], Zhang Deshuai[1,2**], Liu Suping[1], Pan Zhipeng[1,2],
Chang Jinyuan[1,2], He Tianjiang[1,2], Ma Xiaoyu[1,2]

[1]*National Engineering Research Center for Optoelectronic Devices*, *Institute of Semiconductors*, *Chinese Academy of Sciences*, *Beijing* 100083, *China*;

[2]*College of Materials Science and Opto-Electronic Technology*, *University of Chinese Academy of Sciences*, *Beijing* 100049, *China*

Abstract

Objective As the main pumping light source of solid state laser, fiber laser, and fiber amplifier, 976 nm diode laser has been widely used in industrial processing, medical treatment, communication, and other fields. As an important pumping light source of erbium-doped fiber amplifier, a 976 nm fundamental transverse mode diode laser can achieve high-efficiency coupling with fiber, improve the output performance of the fiber amplifier, and effectively reduce the cost of the fiber amplifier. It plays a very important role in improving the application of erbium-doped fiber amplifier in fiber communication and other fields. However, since the ridge waveguide in the ridge diode laser uses the weak refractive index guiding mechanism to suppress the higher-order transverse mode, it will be greatly affected by the lateral diffusion of carriers and the self-heating effect and eventually lead to the decline of the ridge waveguide mode guiding and the increase of the far-field angle. To further improve the coupling efficiency of diode lasers in fiber laser pumping applications and reduce the application cost of fiber lasers, it is still important to realize low far-field divergence angle and low power consumption of fundamental transverse mode ridge diode lasers.

Methods Using InGaAs/GaAsP material as the strain-compensated quantum well structure, and GaAsP with high bandgap width as the barrier material can effectively reduce the carrier leakage effect of quantum well, provide strain compensation for InGaAs compressive strain quantum well, and improve the epitaxial growth quality. To achieve low loss, we optimize high output optical power and low far-field angle, the thickness of waveguide layers by using asymmetric large optical cavity epitaxial structure. The doping concentrations of the epitaxial layer materials are optimized to reduce the series resistance of the device, to achieve high power, high conversion efficiency, and low far-field output of the ridge diode laser. To achieve fundamental transverse mode output, we use the effective refractive index method to design and study the width and depth of the ridge waveguide and map the optical field distribution inside the device. Finally, according to the technological conditions, the ridge waveguide structure is selected with a width of 5 μm and a depth of 0.85 μm.

Results and Discussions After the laser chip is designed and prepared, the output performance of the device is tested at 25 ℃. The device threshold current is about 51.2 mA, and a maximum continuous output power of 422 mW can be obtained at 550 mA injection current, with a maximum electro-optic conversion efficiency of 53.6% (Fig. 3). The peak wavelength is 973.3 nm at 550 mA injection current, and the corresponding spectral line width (FWHM) is 1.4 nm. When the injection current is 500 mA, the vertical and horizontal far-field distribution diagrams of the device are drawn (Fig. 5), and the corresponding vertical and horizontal far-field divergence angles (FWHM) are 24.15° and 3.9°, respectively. This indicates that the prepared ridge diode laser has a good fundamental transverse model property, which is conducive to improving the coupling efficiency between the diode laser and the fiber. Subsequently, we analyze the temperature characteristics of the device at the operating temperature of 15‒35 ℃ and obtain a relatively high characteristic temperature of about 194 K. This is because GaAsP material with high band gap width is added to both sides of the InGaAs quantum well as the barrier layers, and there is a larger band level between the two materials, which can better suppress carrier leakage in the quantum well. The injection current utilization, the luminous efficiency, and the temperature stability of the laser device are improved. Similarly, the horizontal far-field changes little at 15 ℃, 25 ℃, and 35 ℃, and the corresponding horizontal far-field divergence angles are 3.45°, 3.90°, and 3.90°, respectively, which is conducive to increasing the coupling efficiency in optical pumping applications (Fig. 7).

Conclusions We design and fabricate a 976 nm fundamental transverse mode ridge diode laser. To improve the conversion efficiency of the device, we improve high-bandgap GaAsP materials on both sides of the InGaAs compressive strain quantum well as a tensile strain barrier to improve the internal gain of the device, inhibit the carrier leakage in the quantum well, and improve the current utilization rate. In addition, we optimize the waveguide layer thickness and doping concentration in the device epitaxial structure to reduce the far-field divergence angle and achieve high-efficiency output by using an asymmetric large optical cavity epitaxial structure design. A 976 nm strain-compensated low far-field fundamental transverse mode ridge diode laser with a ridge width of 5 μm and a cavity length of 1500 μm is fabricated. At the operating temperature of 25 ℃, the maximum continuous output power of 422 mW can be obtained, the peak wavelength is 973.3 nm, and the spectral line width (FWHM) is 1.4 nm. When the injection current is 500 mA, the vertical and horizontal far-field divergence angles (FWHM) are 24.15° and 3.90°, respectively. In the operating temperature range of 15–35 ℃, the far-field divergence angle of the ridge diode laser is tested and analyzed. It is found that the far-field distribution of the device changes little with the increase in the test temperature, and the far-field divergence angle can be kept small.

Key words lasers; 976 nm diode laser; fundamental transverse mode ridge waveguide; narrow far-field divergence angle; asymmetric large optical cavity structure